

Plasmonic Nanolamination for High-Performance SERS Substrates Based on Vertically Stacked 3D Multiple Nanogaps

Jiwon Yun, Hyeim Yu, and Wonil Nam*

Cite This: *ACS Appl. Nano Mater.* 2025, 8, 5028–5036

Read Online

ACCESS |



Metrics & More



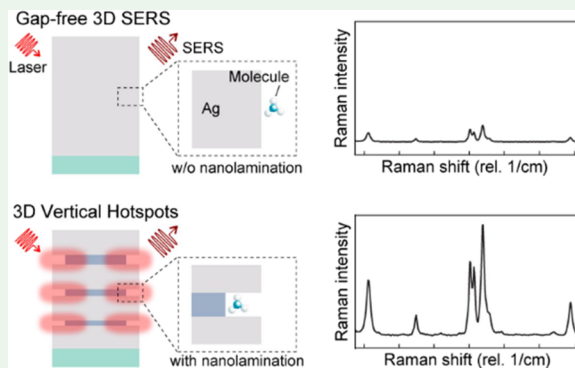
Article Recommendations



Supporting Information

ABSTRACT: While surface-enhanced Raman spectroscopy (SERS) offers ultrasensitive detection performance, achieving signal reproducibility remains a key challenge due to nanoscale geometrical variations in plasmonic hotspots. Top-down fabrication strategies have been employed to improve uniformity and reproducibility; however, the current horizontally oriented nanogaps are limited in achieving precise control at sub-10 nm scales, restricting the achievement of a high density of hotspots. In this work, we report a high-performance silver-based nanolaminate SERS substrate based on vertically stacked 3D multiple nanogaps, providing uniform and densely packed hotspots. By selectively etching the dielectric layers, nanogap hotspots are exposed to analyte molecules, resulting in a significant increase in the SERS enhancement factor, reaching up to 1.75×10^8 . We also demonstrate that plasmonic nanolamination reveals great uniformity with a relative standard deviation value of 11% over a large area (400 pixels) and quantitatively confirms substrate reproducibility. Furthermore, the high-throughput nanoimprint lithography to fabricate high-performance nanolaminate SERS substrates allows the fabrication of large-scale devices ($\sim 16 \text{ cm}^2$) cost-effectively. Therefore, this work presents that the silver-based nanolaminate SERS substrate is highly suitable for various practical SERS applications due to its uniformity, reproducibility, and high sensitivity.

KEYWORDS: surface-enhanced Raman spectroscopy (SERS), high-performance SERS, nanolaminate, nanogaps, plasmonics, wet-etching



INTRODUCTION

Surface-enhanced Raman spectroscopy (SERS) is a powerful technique that can overcome the inherently low scattering efficiency in Raman spectroscopy. Raman scattering containing molecular fingerprint information can be significantly enhanced by a strong electromagnetic (EM) field stemming from plasmon resonance, allowing for expanding the applicability of SERS in various fields. It has emerged as an ultrasensitive technique for detecting and analyzing low-concentration molecules using diverse samples.^{1–6} SERS has been demonstrated as an effective sensing tool, enabling rapid and non-destructive detection, with no requirement for sample pretreatment. As a label-free analytical method, SERS directly provides rich molecular fingerprint information, making it suitable for applications such as environmental contaminants, biosensing, food safety, and the detection of explosives.^{7–14} In the SERS mechanism, the primary one is the EM enhancement that the Raman signal from molecules located near the plasmonic metal surface is greatly enhanced due to the amplification of the EM field. The EM field is significantly amplified through the surface plasmon resonance of the metallic nanostructures via a two-step enhancement process involving both the incident and scattering fields.^{15,16} The spatial region where strongly enhanced electric fields exist is

called a plasmonic hotspot. The SERS enhancement is influenced by the distance between the hotspot and the analytical molecules, as well as the arrangement of hotspots, which is determined by several factors such as size, shape, and material composition of the plasmonic nanostructure.¹⁵ In terms of materials, SERS substrates commonly employ gold and silver, due to their capability to generate a robust local electric field enhancement at visible and near-infrared (NIR) laser wavelengths. Moreover, gold exhibits great biocompatibility as well as remarkable chemical and thermal stability with a slow oxidation rate. Compared to gold, silver is not only more cost-effective but also exhibits relatively stronger plasmonic, leading to higher detection sensitivity.^{17,18}

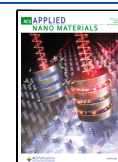
Despite the high sensitivity of SERS, the heterogeneous nature of EM enhancement due to the nanoscale geometrical variations has been identified as a significant limitation; therefore, employing a substrate with uniformly distributed

Received: December 2, 2024

Revised: February 6, 2025

Accepted: February 10, 2025

Published: February 19, 2025



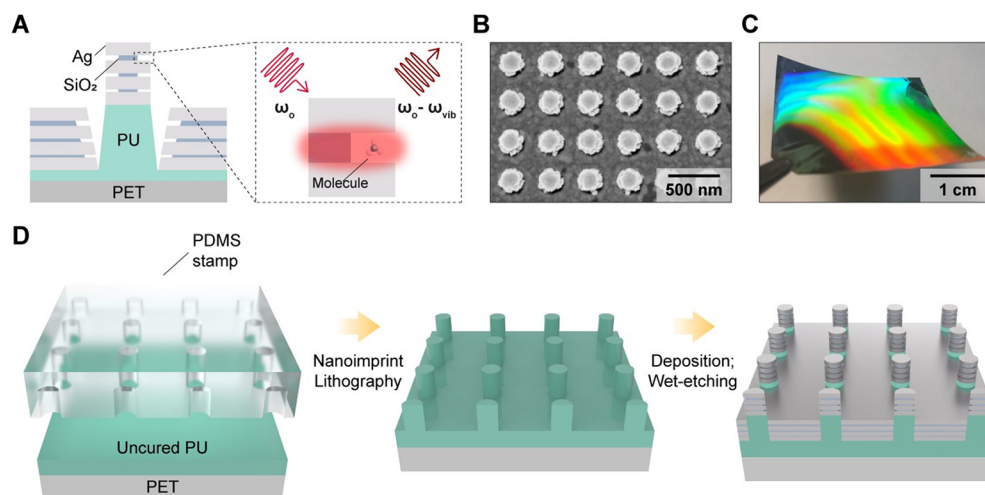


Figure 1. Nanolaminate SERS substrates. (A) Schematic illustration of plasmonic nanolamination over vertical nanopillar structures. (B) A top-view SEM image, (C) a photograph, and (D) fabrication procedures of nanolaminate SERS substrates.

hotspots is essential for precise quantitative analysis.^{19,20} Furthermore, even with great uniformity, achieving reproducible SERS performance has remained challenging, thereby precluding SERS in practical applications. Consequently, the design of SERS substrates has been strategically focused on optimizing nanostructures with precisely arranged nanogaps to simultaneously achieve great uniformity, reproducibility, and maximum EM field enhancement.^{1–3}

Nanogaps in high-performance SERS substrates are generally created by two methods: top-down fabrication and bottom-up synthesis approaches. For decades, great effort has been devoted to both approaches to achieve uniform and highly sensitive hotspot arrays by overcoming their inherent limitations. Despite its high sensitivity and cost-effectiveness in the bottom-up approach, the wet chemistry-based method faces limitations in terms of poor uniformity and reproducibility. These issues arise primarily due to the random aggregation of nanoparticles during self-assembly, making it difficult to control their size, shape, and spatial arrangement precisely. To mitigate large spatial variation of SERS enhancement factor (EF), vertically aligned nanorod/particle arrays that can provide uniform SERS performance have been recently reported by balancing between the concentration of Au nanoparticles and physicochemical parameters of the solvent, which allows the formation of superlattices.^{21–24}

On the other hand, lithography-based top-down procedures can achieve great uniformity and reproducibility by precise control of nanoscale geometrical parameters with advanced techniques such as nanoimprint lithography and laser interference lithography.^{25,26} However, the working volume of the SERS hotspot (sub-10 nm scale) is beyond the resolution limit of typical lithography-based fabrication techniques, therefore, relatively weaker sensitivity has been one of the intrinsic limitations of the top-down approach. High-resolution fabrication techniques such as electron-beam lithography and focused-ion beam (FIB) milling can be used; however, these are inefficient in practical applications due to high costs, time-consuming nature, and low manufacturing yields.^{25–28} To overcome these challenges, block copolymer lithography, which leverages the phenomenon of self-assembly for large-area patterning, has been considered an alternative technique.^{29,30}

Among the various top-down-based strategies, the introduction of 3D vertical nanostructures has emerged as a means to maintain high reproducibility and uniformity while simultaneously forming highly sensitive plasmonic hotspots.^{31–33} Contrary to the 2D planar substrates where the nanogaps are only arranged in-plane,^{34–36} the 3D vertical nanostructures, organized out-of-plane, can further generate plasmonic coupling in the vertical direction, resulting in the expansion of 3D high-density hotspots. One representative is the concept of leaning nanopillar substrates induced by capillary force during the evaporation of solution containing the analyte molecules.^{37–40} The formed nanopillar clusters provide strong lateral coupling among metal-coated vertical nanostructures and can trap the molecules within the generated hotspots. Despite difficulties in dealing with different molecule sizes, affinity, and concentration, it has been recently reported to achieve both high sensitivity and low spatial variation over a 6-in. wafer.⁴¹ However, its versatility is still limited to the dry status of molecules. Other types of 3D SERS substrates where coating metal on vertical nanostructures generates horizontally oriented nanogaps have achieved both high sensitivity and great uniformity over large areas.^{42–44} However, such structures still rely on high-cost and low-throughput fabrication techniques. In addition, changing nanoscale geometry to achieve spectral tunability is challenging while simultaneously retaining highly sensitive sub-10 nm plasmonic hotspots. As an alternative strategy, gap-free SERS substrates have been reported.^{45–49} These quasi-3D plasmonic crystals allow strong vertical coupling between a continuous perforated nanohole array at the base of vertical nanostructures and metallic nanostructures on top of the vertical nanostructures. While the plasmonic resonance wavelength can be easily tuned by adjusting the cavity height with the added advantage of being insensitive to nanogap geometry, the SERS sensitivity is relatively weaker due to the lack of a high density of hotspots. Therefore, it is still a big challenge to satisfy the requirements toward practical SERS applications for both bottom-up and top-down approaches.

Here, we present high-performance SERS substrates based on vertically stacked 3D multiple nanogaps achieved by plasmonic nanolamination of silver-based metal–insulator–metal (MIM) building blocks (Figure 1A). Multiple stacking of such geometry (i.e., nanolamination) allows for creating

plasmonic crystals with multiple resonant optical characteristics and fine-tuning resonant wavelengths.⁵⁰ The plasmonic nanolamination based on multiple MIM configurations can support high-density out-of-plane nanogaps, essential for achieving high SERS performance. Unlike conventional MIM structures, the selectively etched SiO₂ nanogaps provide physical access for target analytes into hotspots with highly enhanced EM fields, leading to a significant improvement in SERS sensitivity. Compared to the gold-based nanolaminate SERS substrates,⁵¹ we observe improved uniformity in silver-based plasmonic nanolamination. Interestingly, silver-based multiple MIM building blocks exhibit qualitatively and quantitatively different optimum etching conditions, which is attributed to the intrinsically different material properties. In this work, we demonstrate that plasmonic nanolamination provides densely packed and uniform arrays of plasmonic hotspots and simultaneously achieves high sensitivity (SERS EF = 1.75×10^8) and great uniformity (relative standard deviation (RSD) = 11.2% from 400 pixels) under optimum etching condition with remarkable reproducibility. The high-throughput nanoimprint lithography technique used to fabricate silver-based plasmonic nanolamination allows the fabrication of large-scale devices (~ 16 cm²) with good reproducibility and the reproducibility was verified by quantitatively analyzing batch variations. Furthermore, the far-field optical property of nanolaminate SERS substrates reveals broadband plasmonic resonance from visible to NIR range, holding great potential in wider SERS applications.

RESULTS AND DISCUSSION

Figure 1B presents a top-view scanning electron microscope (SEM) image showing silver-based nanolaminate SERS substrates with a periodicity of 400 nm. A low-magnification SEM image is shown in Figure S1. To further characterize the substrate with periodic nanopillar structures, atomic force microscopy was performed before metal and oxide deposition (Supporting Information, Figure S2). The resulting strong diffraction patterns captured in the photograph shown in Figure 1C confirm the uniform distribution of periodic nanostructures. This observation supports the feasibility of fabricating SERS substrates at the centimeter scale on flexible substrates. Figure 1D illustrates the top-down fabrication procedure for creating plasmonic nanolamination SERS substrates over vertical nanopillar structures. First, we used a polydimethylsiloxane (PDMS) stamp corrugated with nano-holes to imprint periodic vertical arrays of polyurethane (PU). PU was drop-casted on a flexible polyester (PET) film and cured by UV light. After peeling off the stamp, we deposited alternating layers of Ag (30 nm) and SiO₂ (6, 8, 12 nm from bottom) to achieve plasmonic nanolamination on vertical nanopillars. To activate multiple out-of-plane nanogaps, we used buffered oxide etchant (BOE) for wet-etching of SiO₂ layers (Supporting Information). This simple nanoimprinting procedure allows mass production of high-performance SERS substrates in a high-throughput and cost-effective way with the added advantages of compatibility with flexible and transparent substrates.

Since etching dielectric layers allows molecules to physically approach high enhancement nanogap hotspot regions, which were initially inaccessible for them, we measured SERS spectra of benzenethiol (BZT) self-assembled monolayer (SAM), a non-resonant Raman analyte, with different BOE etching times under 785 nm excitation. Figure 2 shows the average Raman

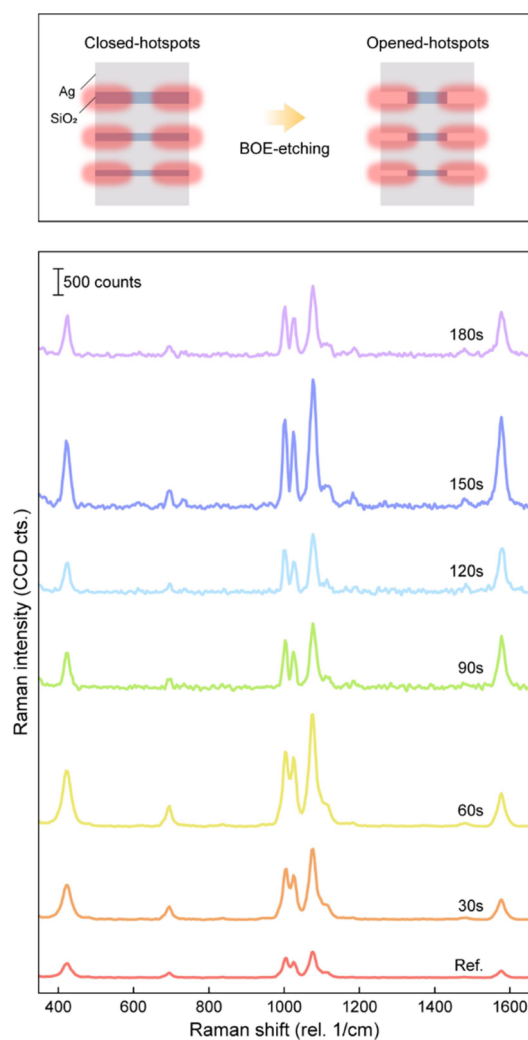


Figure 2. Measured SERS performance of nanolaminate SERS substrates. 2D schematic illustration of the nanolaminate substrate before and after BOE etching (top). Measured average SERS spectra of BZT molecules under 785 nm excitation with different etching conditions from non-etched to 180 s-etched with increments of 30 s (bottom).

intensities of BZT molecules ($n = 400$) with different etching times from 0 to 180 s with 30 s increments and the major peaks observed are well-matched with the known signature peaks of BZT.⁵² The primary peaks at 420, 1002, 1024, 1076, and 1577 cm⁻¹ are attributed to distinct vibrational modes in BZT molecules, corresponding the carbon–sulfur (C–S) stretching and carbon–carbon–carbon (C–C–C) ring in-plane deformation vibration, the C–C–C ring in-plane bending mode, the carbon–hydrogen (C–H) in-plane bending mode, the C–C–C ring in-plane breathing mode coupled with the C–S stretching mode, and the C–C stretching mode.⁵² As the etching time increases from 0 to 120 s, the intensities gradually increase and then decrease with the highest intensity at the 60 s-etched sample. The Raman intensities of characteristic vibrational modes observed at peaks 420, 1002, 1024, 1076, and 1577 cm⁻¹ for the non-etched spectra are 265, 370, 299, 493, and 1577, respectively. For the 60 s-etched spectra, the Raman intensities at each peak are 1070, 1435, 1328, 2153, and 633, respectively. The 60 s-etched one shows up to 4.4 times higher intensity than the non-etched

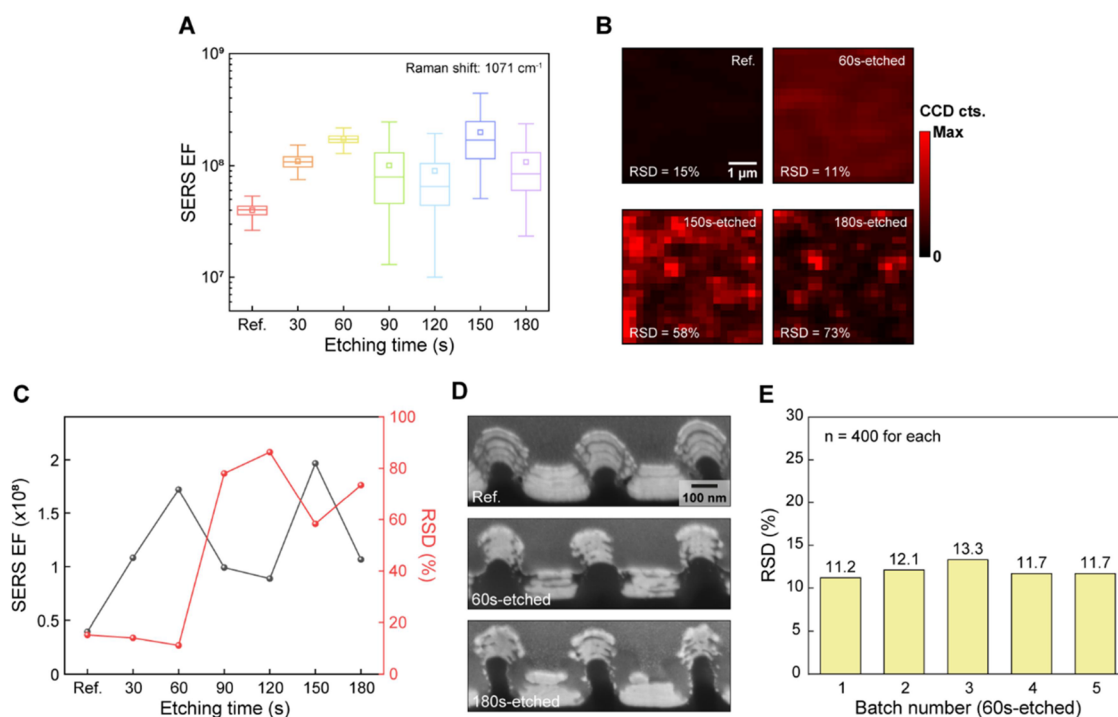


Figure 3. SERS performance of nanolaminate SERS substrates. (A) Calculated SERS EFs from the measured data as a function of etching time. A Raman shift of 1071 cm^{-1} was used. (B) $5 \mu\text{m} \times 5 \mu\text{m}$ 2D Raman images of four different etching conditions with their RSD values. (C) Average SERS EFs and RSDs of nanolaminate SERS substrates with different etching conditions. (D) Cross-sectional FIB-SEM images of plasmonic nanolamination with different etching conditions. (E) Reproducibility assessment of 60 s-etched nanolaminate SERS substrates using five different batches.

one, and over-etching seems to degrade SERS performance due to geometrical deformation of plasmonic nanolamination. Remarkably, additional etching from 120 s makes intensities higher again and then lower rather than gradually decreasing. For instance, the 150s-etched sample provides the highest SERS sensitivity, 5-fold of the non-etched one. However, the uniformity of hotspots is significantly degraded, which will be discussed.

In Figure 3A, we delve deeper into the SERS performance of nanolaminate substrates under various etching conditions, calculating SERS EFs using the formula $EF = (I_{\text{SERS}}/I_{\text{Raman}}) \times (N_{\text{Raman}}/N_{\text{SERS}})^{53}$ (Supporting Information). Figure 3A shows the calculated SERS EFs with different etching conditions and $1.5 \times$ interquartile range (IQR) which indicates the uniformity of SERS substrates. As etching time increases from 0 to 60 s, SERS EFs exhibit an increasing trend with the maximum value (1.75×10^8) at 60 s etching. From 60 s, the decreasing trend is observed with an abrupt increase at 150 s. Although the 150 s-etched sample exhibits the highest SERS EF of 2×10^8 , it shows a much broader EF distribution compared to the 60 s-etched one. Furthermore, by observing the error bars for samples including 60, 90, 120, 150, and 180 s-etched substrates, it is more evident that over-etching results in the deformation of plasmonic nanolamination and thereby collapse of vertically stacked 3D multiple nanogaps. An abrupt increase of SERS EF in the 150 s-etched sample is attributed to the randomly formed additional plasmonic hotspots from the collapsed nanostructures.

To study the etching effect on the uniformity of SERS substrates, 2D Raman images over $5 \mu\text{m} \times 5 \mu\text{m}$ area with etching times of 0, 60, 150, and 180 s are plotted (Figure 3B) using a Raman shift of 1071 cm^{-1} . The mapping area was

determined by considering a periodicity of 400 nm, and a calculated laser spot size of 1064 nm. The 1064 nm laser spot size was selected to enable precise analysis of individual MIM building blocks by minimizing the spot size. This reduction in spot size decreases the number of MIM structures within the illuminated laser spot, facilitating a more detailed and accurate investigation of individual MIM blocks. In this way, we can evaluate the uniformity of MIM building blocks with a stricter condition, resulting in a higher RSD value. Consequently, the laser spot size of 1064 nm ensures that an individual nanolaminate structure resides within 50% of the laser power distribution limit set by the Airy disk diffraction pattern, allowing for precise evaluation of uniformity across vertically stacked MIM building blocks. Between the non-etched (Ref.) and 60 s-etched samples, we observed a similar level of RSDs (15.2 and 11.2%), while the samples etched with 150 and 180 s show dramatically increased RSDs (58.3 and 73.5%) with high spatial variations over 2D maps indicating that over-etching degrades the uniformity of SERS hotspots. To further assess uniformity over a relatively larger area, we performed 2D mapping using the 60 s-etched sample with an area of $10 \mu\text{m} \times 10 \mu\text{m}$, including 400 pixels (Figure S3, Supporting Information). The calculated RSD values are 9.7, 11.8, and 11.7%, comparable or lower compared to the $5 \mu\text{m} \times 5 \mu\text{m}$ mapping results. Figure 3C shows average SERS EFs and RSDs as a function of BOE etching time and we performed FIB milling SEM to visually investigate the etching effect on the geometry of plasmonic nanolamination as shown in Figure 3D. As the etching time increases, the RSD values do not change dramatically until 60 s, however, it abruptly increases up to 86.3% (120 s-etched) with etching times over 90 s. The observed trend including the results of 2D Raman mapping is

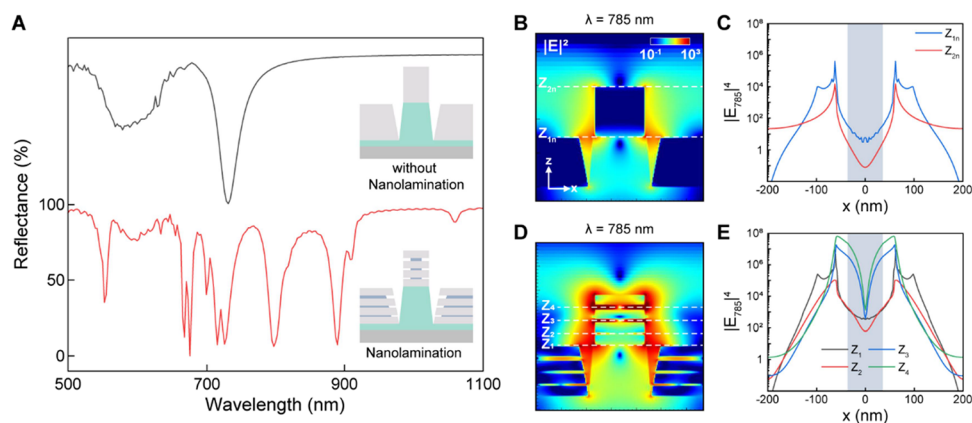


Figure 4. Far-/near-field optical properties of nanolaminate SERS substrates. (A) FDTD-calculated reflectance spectra of nanopillars without (top, black) and with (bottom, red) plasmonic nanolamination. Inset images show schematic illustrations of two structures. The spectrum has been displaced by 100% for clarity. (B, D) FDTD-calculated distribution maps of $|E|^2$ at the excitation wavelength 785 nm. Different z -positions in Figure 4C,E are indicated as dashed white lines. Calculated $|E|^4$ of (C) typical gap-free structure and (E) plasmonic nanolamination at different z -positions.

confirmed by FIB-assisted cross-sectional SEM images that the 60 s-etched sample (Figure 3D, middle) retains the initially designed plasmonic nanolamination geometry compared to the non-etched sample (Figure 3D, top) whereas the 180 s-etched sample (Figure 3D, bottom) no longer reveals clear plasmonic nanolamination with irregular metal shape and partially collapsed nanostructures. Over-etching makes the insulator layers thinner, and the mechanically weakened layers no longer support vertically stacked structures. The increased RSD value from 90 to 120 s reflects a progressive structural collapse. At 120 s, over-etching peaked, causing severe structural degradation, thereby the maximum RSD value. Therefore, the abrupt increase of SERS EF at 150 s etching is highly likely due to the additionally generated random hotspots providing strong enhancement from collapsed structures by over-etching. Interestingly, such an optimal etching condition trend is both quantitatively and qualitatively different from the previous studies that the etching effect of gold-based plasmonic nanolamination shows a linear increasing and decreasing trend with only one optimum condition (30 s-etched).⁵¹ Moreover, for the optimized structures, silver-based nanolamination reveals improved uniformity (silver-based RSD: 11% and gold-based RSD: 28%), and such differences are attributed to the intrinsically different material properties between gold and silver. First, gold is known for being softer and tends to combine each other which may not generate additional nanogaps or plasmonic hotspots by over-etching. Second, silver is relatively more rigid; therefore, the nanostructures may preserve better their original geometries after wet-etching. In terms of sensitivity, silver-based plasmonic nanolamination shows a similar level of SERS EF to gold-based nanolamination, due to their comparable plasmon efficiency under 785 nm excitation.⁵⁴ Theoretically, silver-based SERS substrates are expected to produce higher EFs under visible excitation compared to other metals, supporting their superior enhancement capability.^{17,18}

We then investigated the reproducibility of nanolaminate SERS substrates by quantitatively assessing the batch variation of 60 s-etched substrates across five different batches, all processed under identical conditions (each measured over a $5 \mu\text{m} \times 5 \mu\text{m}$ area with 400 pixels). Figure 3E shows a bar graph of RSD values that can quantify the uniformity of plasmonic hotspots. We used a Raman shift of 1071 cm^{-1} and the RSD

values from five SERS substrates are 11.2, 12.1, 13.3, 11.7, and 11.7%, respectively, confirming the great reproducibility of nanolaminate SERS substrate fabrication. To additionally assess fabrication reproducibility, we conducted a batch variation study by calculating RSD values of 150 s- and 180 s-etched substrates (Figure S4, Supporting Information). The three different samples for each etching condition exhibit similar uniformity degradation trends after over-etching. Specifically, for the 150 s-etched substrates, the RSD values are 58.3, 51.5, and 57.6%, and for the 180 s-etched substrates, the RSD values are 73.5, 77.8, and 78.4%, confirming the above statement that over-etching causes the collapse of nanostructures and increases the randomness of hotspots. These batch variation results support the excellent consistency of the nanolaminate SERS substrate fabrication recipe including the nanoimprint lithography technique. Therefore, nanolaminate SERS substrate assessment in Figure 3 indicates that the 60 s-etched plasmonic nanolamination provides high SERS performance in terms of sensitivity (1.75×10^8) and uniformity (RSD = 11%) with remarkable reproducibility.

To understand the effect of plasmonic nanolamination, we performed a 3D finite-difference time-domain (FDTD) calculation and compared far-/near-field optical properties of structure with and without plasmonic nanolamination schematically illustrated as the insets in Figure 4A. Figure 4A shows the FDTD-calculated reflectance spectra of SERS substrates without (top, black) and with (bottom, red) plasmonic nanolamination. For the case of without plasmonic nanolamination which is typically called as gap-free SERS substrates, it shows one distinct reflection dip at 730 nm. To estimate SERS performance, we calculated near-field optical properties of the electric field intensities ($|E|^2$) at the excitation wavelength (785 nm). The major optical field confinement occurs between the top metallic structure and bottom nanohole arrays through coupling and the edges of the top metallic structure partially contribute (Figure 4B). As shown in Figure 4C ($|E|^4$ along the x -axis), the enhanced fields are only observed at the surface and rapidly decrease as they extend away from the surface. Based on the $|E|^4$ approximation,⁵³ The estimated SERS EF is 4×10^5 at the plasmonic coupling region, which is in good agreement with the SERS EF values of the reported gap-free structures.^{45,46}

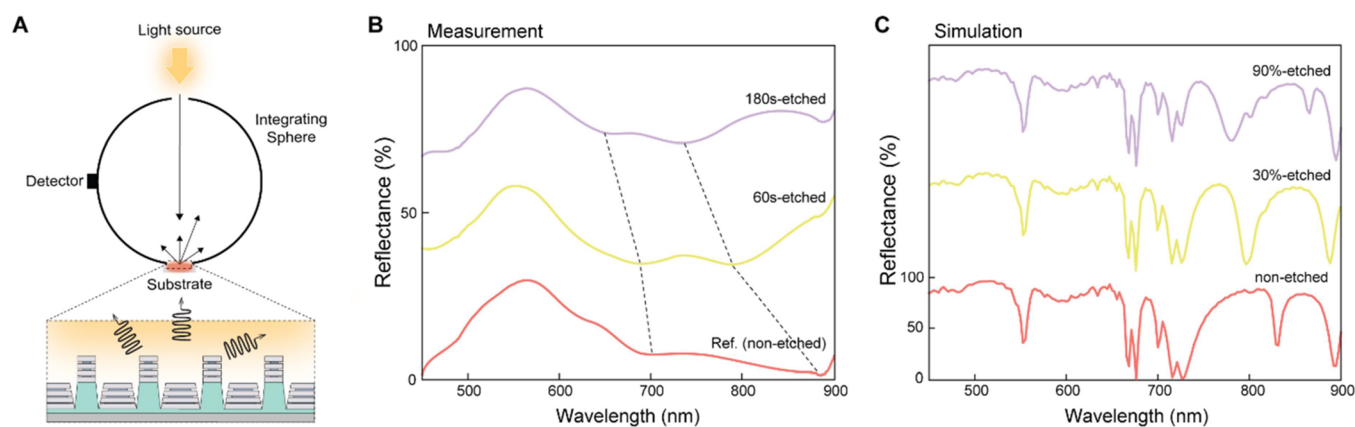


Figure 5. Optical properties of nanolaminate SERS substrates. (A) Experimental configuration of reflectance measurement utilizing an integrating sphere. (B) Measured and (C) simulated reflectance spectra of nanolaminate SERS substrates with three different etching conditions. The individual spectra have been displaced by 30 (measurement) and 100% (simulation) for clarity.

In contrast, the adoption of plasmonic nanolamination can provide multiresonant optical property featured by several reflectance dips (Figure 4A). Briefly, the underlying physics of the additional reflectance dips observed from the nanolaminate structure is due to the generation of gap plasmons. The nanolaminate structure, containing three insulator layers with thicknesses of 6, 8, and 12 nm, exhibits corresponding localized surface plasmon resonances at 800, 890, and 1060 nm, respectively. Compared to the case without nanolamination (i.e., gap-free structure) with one distinct reflection dip at 730 nm, the nanolaminate structure reveals several additional neighboring dips that originate from delocalized plasmonic modes in the base MIM nanolaminate nanohole arrays and near-field optical hybridization between localized and delocalized plasmonic modes. The calculated electric field intensity map (Figure 4D) shows much stronger fields confined in the out-of-plane nanogaps as well as stronger coupling between nanolaminate structures on top of and on the base of vertical nanopillars. In Figure 4E, compared to Figure 4C, the highly enhanced fields are observed within the closed nanogap region (gray) as additional hotspots are generated, reaching its maximum at the opened nanogap regions before rapidly decreasing outside the nanogap region. The estimated SERS EF of the nanolaminate SERS substrates is 6.5×10^7 from the top nanogap, which is slightly lower than the measured SERS EF of 1.75×10^8 using BZT SAM and it is attributed to the surface roughness not taken into account in the simulation.

To investigate the far-field optical property of nanolaminate SERS substrates and the effect of the wet-etching process, we measured reflectance spectra with different etching times. Figure 5A illustrates the reflectance measurement configuration using a UV–vis–NIR spectrophotometer equipped with an integrating sphere that can collect both specular and diffuse reflectance. As shown in Figure 5B, the non-etched sample (Ref.) reveals low reflectance (1–25%) over a wide range from 400 to 900 nm with multiresonant optical property. Multiple spectrally overlapped reflectance dips induced by the absorption of different plasmonic modes are featured at roughly 625, 705, and 880 nm. Figure 5C shows FDTD-calculated reflectance spectra of nanolaminate SERS substrates with different etching conditions, including non-etched, 30%-etched, and 90%-etched (see Figure S5 for simulation profiles of the corresponding models) to realize the BOE-etched

samples similarly. By comparing the reflectance spectra between measurement and simulation results, we can confirm that the positions of reflectance dips are qualitatively well-matched (Figure S6). The differences between simulation and measurement in terms of the number of reflectance dips and resonant width are due to the inhomogeneous broadening effect from geometrical variations between individual nanolaminate structures and the homogeneous broadening effect from additional optical losses due to metal-dielectric interface roughness and nanocrystalline boundaries in the metal layers.^{55,56} After etching for 60 and 180 s, the broad dips in the reflectance spectra reveal blue-shifting. This blue-shift trend can be explained by the relationship between the refractive index and the position of surface plasmon resonance (SPR), described in terms of the dielectric constant of the medium and the SPR wavelength. According to this relationship, as the effective refractive index decreases, the resonance wavelength shifts to shorter wavelengths. More specifically, the two broad dips initially at 705 and 880 nm are blue-shifted to 690 and 790 nm for 60 s, and to 655 and 735 nm for 180 s BOE etching, respectively. The reflectance dip amplitudes and widths for the non-etched, 60 s-etched, and 180 s-etched samples show no significant change after the etching due to the collective blue-shifting of multiple resonances that are compositions of the broad resonance. Compared to the measurement results, the simulation results exhibit a similar trend that reflection dips are blue-shifted as the extent of etching increases, initially observed at 830 nm (non-etched), to 800 nm (30% etched), and 780 nm (90% etched). While the overall trend of blue-shifting is qualitatively consistent, the calculated results for resonance wavelengths and reflectance dip amplitudes are noticeably different from the experimental results. Such inconsistency may stem from the fact that the FDTD simulation model cannot effectively account for surface roughness and the geometric deformations induced by the BOE etching process. Computational findings reveal much slighter alterations in resonant wavelengths and reflectance dip amplitudes; however, the experimental results exhibit broadband resonance from visible to NIR region while retaining a qualitative blue-shift trend resulting from the reduction in effective refractive index. The reflectance results confirm that nanolaminate SERS substrates can cover both excitation wavelength and the Stokes-Raman scattering range. We believe that such broadband and high-performance SERS substrates

with multiple 3D nanogaps are versatile and may play a significant role in the SERS field.

CONCLUSIONS

In summary, we demonstrate plasmonic nanolamination over vertical nanopillar structures that can support a high density of 3D nanogaps, enabling high SERS performance. In the design of SERS substrates, great uniformity and reproducibility have been generally achieved by gap-free SERS substrates; however, plasmonic nanolamination with the optimum wet-etching condition yields more than 2 orders of magnitude higher SERS EF (1.75×10^8) than those of typical gap-free structures ($\sim 4 \times 10^5$), i.e., without nanolamination, while preserving both uniformity and reproducibility. We systematically studied SERS performance by controlling the degree of opening nanogaps, thereby physically exposing hotspots, and showed that the over-etching process induces significant degradation of SERS uniformity, supported by FIB-SEM images. Compared to the gold-based substrates at the optimal condition, silver-based substrates demonstrate a lower RSD of 11%, indicating that the silver structures are less mechanically susceptible to degradation while preserving their original nanoscale geometries due to their relatively higher material rigidity. Such observations can be helpful information for designing gap-based SERS substrates. Measured and FDTD-calculated optical properties reveal that nanolaminate structures can support multiple plasmonic modes originating from the vertically stacked multiple MIM building blocks and provide strong field enhancement. Furthermore, the nanolaminate SERS substrates can be fabricated in a high-throughput and cost-effective way over a large area with great reproducibility. Furthermore, a recent study showed that the plasmon resonance wavelengths of such nanolaminate structures can be straightforwardly tuned by controlling the dielectric layer thicknesses.⁵⁰ Therefore, we believe that high-performance nanolaminate SERS substrates are well-suited for practical SERS applications.

ASSOCIATED CONTENT

Supporting Information

The Supporting Information is available free of charge at <https://pubs.acs.org/doi/10.1021/acsanm.4c06770>.

Nanolaminate SERS substrate fabrication; SERS EF calculation; BOE for wet-etching of the SiO₂ layer; SERS measurement; reflectance measurement; FDTD simulation; top-view SEM image of the nanolaminate SERS substrates; 2D AFM image of the substrate before deposition; 10 μm × 10 μm 2D Raman images with RSD values; RSD values for over-etched (150 and 180 s) nanolaminate SERS substrates at 1071 cm⁻¹; simulation models of non-, 30%, and 90%-etched conditions; and measured and simulated reflectance spectra of nanolaminate SERS substrates (PDF)

AUTHOR INFORMATION

Corresponding Author

Wonil Nam – Department of Electronic Engineering, Pukyong National University, Busan 48513, Republic of Korea;
orcid.org/0000-0002-7804-3049; Email: nam@pknu.ac.kr

Authors

Jiwon Yun – Department of Electronic Engineering, Pukyong National University, Busan 48513, Republic of Korea
Hyeim Yu – Department of Electronic Engineering, Pukyong National University, Busan 48513, Republic of Korea

Complete contact information is available at:
<https://pubs.acs.org/doi/10.1021/acsanm.4c06770>

Author Contributions

J.Y. and H.Y. contributed equally to this work.

Notes

The authors declare no competing financial interest.

ACKNOWLEDGMENTS

This work was supported by the Pukyong National University Industry-University Cooperation Research Fund in 202311710001.

REFERENCES

- (1) Ding, S. Y.; Yi, J.; Li, J. F.; Ren, B.; Wu, D. Y.; Panneerselvam, R.; Tian, Z. Q. Nanostructure-based plasmon-enhanced Raman spectroscopy for surface analysis of materials. *Nat. Rev. Mater.* **2016**, *1* (6), 1–16.
- (2) Han, X. X.; Rodriguez, R. S.; Haynes, C. L.; Ozaki, Y.; Zhao, B. Surface-enhanced Raman spectroscopy. *Nat. Rev. Methods Primers* **2021**, *1* (1), 87.
- (3) Langer, J.; Jimenez de Aberasturi, D.; Aizpurua, J.; Alvarez-Puebla, R. A.; Auguie, B.; Baumberg, J. J.; Bazan, G. C.; Bell, S. E.; Boisen, A.; Brolo, A. G. Present and future of surface-enhanced Raman scattering. *ACS Nano* **2019**, *14* (1), 28–117.
- (4) Nam, W.; Ren, X.; Tali, S. A. S.; Ghassemi, P.; Kim, I.; Agah, M.; Zhou, W. Refractive-index-insensitive nanolaminated SERS substrates for label-free Raman profiling and classification of living cancer cells. *Nano Lett.* **2019**, *19* (10), 7273–7281.
- (5) Zhang, T.; Sun, Y.; Hang, L.; Li, H.; Liu, G.; Zhang, X.; Lyu, X.; Cai, W.; Li, Y. Periodic porous alloyed Au–Ag nanosphere arrays and their highly sensitive SERS performance with good reproducibility and high density of hotspots. *ACS Appl. Mater. Interfaces* **2018**, *10* (11), 9792–9801.
- (6) Zhang, H.; Liu, M.; Zhou, F.; Liu, D.; Liu, G.; Duan, G.; Cai, W.; Li, Y. Physical deposition improved SERS stability of morphology controlled periodic micro/nanostructured arrays based on colloidal templates. *Small* **2015**, *11* (7), 844–853.
- (7) Ong, T. T. X.; Blanch, E. W.; Jones, O. A. H. Surface Enhanced Raman Spectroscopy in environmental analysis, monitoring and assessment. *Sci. Total Environ.* **2020**, *720*, No. 137601.
- (8) Zong, C.; Xu, M.; Xu, L. J.; Wei, T.; Ma, X.; Zheng, X. S.; Hu, R.; Ren, B. Surface-enhanced Raman spectroscopy for bioanalysis: reliability and challenges. *Chem. Rev.* **2018**, *118* (10), 4946–4980.
- (9) Gillibert, R.; Huang, J. Q.; Zhang, Y.; Fu, W. L.; de La Chapelle, M. L. Explosive detection by surface enhanced Raman scattering. *TrAC, Trends Anal. Chem.* **2018**, *105*, 166–172.
- (10) Cao, A.; Zhang, T.; Liu, D.; Xing, C.; Zhong, S.; Li, X.; Zeng, P.; Li, Y. Electrostatic self-assembly of 2D Janus PS@ Au nanoraspberry photonic-crystal array with enhanced near-infrared SERS activity. *Mater. Adv.* **2022**, *3* (3), 1512–1517.
- (11) Chen, Z.; Zeng, P.; Wang, Y.; Zhang, G.; Yu, J.; Cao, A.; Liu, D.; Li, Y. A high-density Ag nanoneedle forest array by using a nano-peeling technique for near-infrared SERS detection. *J. Mater. Chem. C* **2023**, *11* (46), 16195–16200.
- (12) Li, X.; Zhang, T.; Chen, Z.; Yu, J.; Cao, A.; Liu, D.; Cai, W.; Li, Y. Au polyhedron array with tunable crystal facets by PVP-assisted thermodynamic control and its sharp shape as well as high-energy exposed planes Co-boosted SERS activity. *Small* **2022**, *18* (4), No. 2105045.

- (13) Zhao, Y. X.; Liang, X.; Chen, Y. L.; Chen, Y. T.; Ma, L.; Ding, S. J.; Chen, X. B.; Wang, Q. Q. Open-Nanogap-Induced Strong Electromagnetic Enhancement in Au/AgAu Monolayer as a Stable and Uniform SERS Substrate for Ultrasensitive Detection. *Anal. Chem.* **2024**, *96*, 8416–8423.
- (14) Peng, X.; Cheng, X.; Wei, C.; Wan, S.; Ni, K.; Niu, Z.; Han, Y.; Jiang, Z.; Cao, Z.; Shao, J. Laser-based defect characterization and removal process for manufacturing fused silica optic with high ultraviolet laser damage threshold. *Light: Adv. Manuf.* **2023**, *4* (3), 181–194.
- (15) Ding, S. Y.; You, E. M.; Tian, Z. Q.; Moskovits, M. Electromagnetic theories of surface-enhanced Raman spectroscopy. *Chem. Soc. Rev.* **2017**, *46* (13), 4042–4076.
- (16) Le Ru, E. C.; Auguié, B. Enhancement factors: A central concept during 50 years of surface-enhanced Raman spectroscopy. *ACS Nano* **2024**, *18* (14), 9773–9783.
- (17) Sharma, B.; Frontiera, R. R.; Henry, A.-I.; Ringe, E.; Van Duyne, R. P. SERS: Materials, applications, and the future. *Mater. Today* **2012**, *15* (1–2), 16–25.
- (18) Sharma, B.; Cardinal, M. F.; Kleinman, S. L.; Greeneltch, N. G.; Frontiera, R. R.; Blaber, M. G.; Schatz, G. C.; Van Duyne, R. P. High-performance SERS substrates: Advances and challenges. *MRS Bull.* **2013**, *38* (8), 615–624.
- (19) Bell, S. E.; Charron, G.; Cortés, E.; Kneipp, J.; de la Chapelle, M. L.; Langer, J.; Procházka, M.; Tran, V.; Schlücker, S. Towards reliable and quantitative surface-enhanced Raman scattering (SERS): from key parameters to good analytical practice. *Angew. Chem., Int. Ed.* **2020**, *59* (14), 5454–5462.
- (20) Chen, H. Y.; Lin, M. H.; Wang, C. Y.; Chang, Y. M.; Gwo, S. Large-scale hot spot engineering for quantitative SERS at the single-molecule scale. *J. Am. Chem. Soc.* **2015**, *137* (42), 13698–13705.
- (21) Bodelón, G.; Montes-García, V.; López-Puente, V.; Hill, E. H.; Hamon, C.; Sanz-Ortiz, M. N.; Rodal-Cedeira, S.; Costas, C.; Celiksoy, S.; Pérez-Juste, I. Detection and imaging of quorum sensing in *Pseudomonas aeruginosa* biofilm communities by surface-enhanced resonance Raman scattering. *Nat. Mater.* **2016**, *15* (11), 1203–1211.
- (22) Liang, Y.; Xie, Y.; Chen, D.; Guo, C.; Hou, S.; Wen, T.; Yang, F.; Deng, K.; Wu, X.; Smalyukh, I. I. Symmetry control of nanorod superlattice driven by a governing force. *Nat. Commun.* **2017**, *8* (1), 1410.
- (23) Matricardi, C.; Hanske, C.; Garcia-Pomar, J. L.; Langer, J.; Mihi, A.; Liz-Marzán, L. M. Gold nanoparticle plasmonic superlattices as surface-enhanced Raman spectroscopy substrates. *ACS Nano* **2018**, *12* (8), 8531–8539.
- (24) Zhou, Z. R.; Liu, W. X.; Yao, Z. Y.; Zheng, Z. X.; Ma, L.; Chen, X. B.; Ding, S. J. Uniform and Dense Hotspots in Au Rough-Nanocube Monolayer for Sensitive and Reproducible SERS Detection. *ACS Appl. Nano Mater.* **2024**, *7* (14), 17009–17016.
- (25) Jeon, T. Y.; Kim, D. J.; Park, S. G.; Kim, S. H.; Kim, D. H. Nanostructured plasmonic substrates for use as SERS sensors. *Nano Converg.* **2016**, *3*, 18.
- (26) Yang, Y.; Gu, C.; Li, J. Sub-5 nm metal nanogaps: physical properties, fabrication methods, and device applications. *Small* **2019**, *15* (5), No. 1804177.
- (27) Zhang, C.; Li, C.; Yu, J.; Jiang, S.; Xu, S.; Yang, C.; Liu, Y. J.; Gao, X.; Liu, A.; Man, B. SERS activated platform with three-dimensional hot spots and tunable nanometer gap. *Sens. Actuators B* **2018**, *258*, 163–171.
- (28) Piniard, M.; Sorrente, B.; Hug, G.; Picart, P. Melt pool monitoring in laser beam melting with two-wavelength holographic imaging. *Light: Adv. Manuf.* **2022**, *3* (1), 14–25.
- (29) Akinoglu, G. E.; Mir, S. H.; Gatensby, R.; Rydzek, G.; Mokarian-Tabari, P. Block copolymer derived vertically coupled plasmonic arrays for surface-enhanced Raman spectroscopy. *ACS Appl. Mater. Interfaces* **2020**, *12* (20), 23410–23416.
- (30) Jin, H. M.; Kim, J. Y.; Heo, M.; Jeong, S. J.; Kim, B. H.; Cha, S. K.; Han, K. H.; Kim, J. H.; Yang, G. G.; Shin, J. Ultralarge area sub-10 nm plasmonic nanogap array by block copolymer self-assembly for reliable high-sensitivity SERS. *ACS Appl. Mater. Interfaces* **2018**, *10* (51), 44660–44667.
- (31) Dipalo, M.; Messina, G. C.; Amin, H.; La Rocca, R.; Shalabaeva, V.; Simi, A.; Maccione, A.; Zilio, P.; Berdondini, L.; De Angelis, F. 3D plasmonic nanoantennas integrated with MEA biosensors. *Nanoscale* **2015**, *7* (8), 3703–3711.
- (32) Jeong, J. W.; Arnob, M. M. P.; Baek, K. M.; Lee, S. Y.; Shih, W. C.; Jung, Y. S. 3D cross-point plasmonic nanoarchitectures containing dense and regular hot spots for surface-enhanced Raman spectroscopy analysis. *Adv. Mater.* **2016**, *28* (39), 8695–8704.
- (33) He, J.; Shen, Q.; Yang, S.; He, G.; Tao, P.; Song, C.; Wu, J.; Deng, T.; Shang, W. Coupling effects in 3D plasmonic structures templated by Morpho butterfly wings. *Nanoscale* **2018**, *10* (2), 533–537.
- (34) Glangchai, L. C.; Calderera-Moore, M.; Shi, L.; Roy, K. Nanoimprint lithography based fabrication of shape-specific, enzymatically-triggered smart nanoparticles. *J. Controlled Release* **2008**, *125* (3), 263–272.
- (35) Barcelo, S. J.; Kim, A.; Wu, W.; Li, Z. Fabrication of deterministic nanostructure assemblies with sub-nanometer spacing using a nanoimprinting transfer technique. *ACS Nano* **2012**, *6* (7), 6446–6452.
- (36) Das, G.; Chirumamilla, M.; Toma, A.; Gopalakrishnan, A.; Zaccaria, R. P.; Alabastri, A.; Leoncini, M.; Di Fabrizio, E. Plasmon based biosensor for distinguishing different peptides mutation states. *Sci. Rep.* **2013**, *3* (1), 1792.
- (37) Chandra, D.; Yang, S. Capillary-force-induced clustering of micropillar arrays: is it caused by isolated capillary bridges or by the lateral capillary meniscus interaction force? *Langmuir* **2009**, *25* (18), 10430–10434.
- (38) Duan, H.; Berggren, K. K. Directed self-assembly at the 10 nm scale by using capillary force-induced nanocoherence. *Nano Lett.* **2010**, *10* (9), 3710–3716.
- (39) Lao, Z.; Zheng, Y.; Dai, Y.; Hu, Y.; Ni, J.; Ji, S.; Cai, Z.; Smith, Z. J.; Li, J.; Zhang, L. Nanogap plasmonic structures fabricated by switchable capillary-force driven self-assembly for localized sensing of anticancer medicines with microfluidic SERS. *Adv. Funct. Mater.* **2020**, *30* (15), No. 1909467.
- (40) Hu, M.; Ou, F. S.; Wu, W.; Naumov, I.; Li, X.; Bratkovsky, A. M.; Williams, R. S.; Li, Z. Gold nanofingers for molecule trapping and detection. *J. Am. Chem. Soc.* **2010**, *132* (37), 12820–12822.
- (41) Schmidt, M. S.; Hübner, J.; Boisen, A. Large area fabrication of leaning silicon nanopillars for surface enhanced Raman spectroscopy. *Adv. Mater.* **2012**, *24* (10), OP11–OP18.
- (42) Zhang, X.; Zheng, Y.; Liu, X.; Lu, W.; Dai, J.; Lei, D. Y.; MacFarlane, D. R. Hierarchical porous plasmonic metamaterials for reproducible ultrasensitive surface-enhanced Raman spectroscopy. *Adv. Mater.* **2015**, *27* (6), 1090–1096.
- (43) Suresh, V.; Ding, L.; Chew, A. B.; Yap, F. L. Fabrication of large-area flexible SERS substrates by nanoimprint lithography. *ACS Appl. Nano Mater.* **2018**, *1* (2), 886–893.
- (44) Kanipe, K. N.; Chidester, P. P. F.; Stucky, G. D.; Moskovits, M. Large format surface-enhanced Raman spectroscopy substrate optimized for enhancement and uniformity. *ACS Nano* **2016**, *10* (8), 7566–7571.
- (45) Liu, B.; Yao, X.; Chen, S.; Lin, H.; Yang, Z.; Liu, S.; Ren, B. Large-area hybrid plasmonic optical cavity (HPOC) substrates for surface-enhanced Raman spectroscopy. *Adv. Funct. Mater.* **2018**, *28* (43), No. 1802263.
- (46) Huang, J. A.; Zhao, Y. Q.; Zhang, X. J.; He, L. F.; Wong, T. L.; Chui, Y. S.; Zhang, W. J.; Lee, S. T. Ordered Ag/Si nanowires array: wide-range surface-enhanced Raman spectroscopy for reproducible biomolecule detection. *Nano Lett.* **2013**, *13* (11), 5039–5045.
- (47) Xu, J.; Guan, P.; Kvasnička, P.; Gong, H.; Homola, J. i.; Yu, Q. Light transmission and surface-enhanced Raman scattering of quasi-3D plasmonic nanostructure arrays with deep and shallow Fabry-Perot nanocavities. *J. Phys. Chem. C* **2011**, *115* (22), 10996–11002.
- (48) Luo, X.; Jiang, L.; Kang, T.; Xing, Y.; Zheng, E.; Wu, P.; Cai, C.; Yu, Q. Label-free Raman observation of TET1 protein-mediated

epigenetic alterations in DNA. *Anal. Chem.* **2019**, *91* (11), 7304–7312.

(49) Chanda, D.; Shigeta, K.; Truong, T.; Lui, E.; Mihi, A.; Schulmerich, M.; Braun, P. V.; Bhargava, R.; Rogers, J. A. Coupling of plasmonic and optical cavity modes in quasi-three-dimensional plasmonic crystals. *Nat. Commun.* **2011**, *2* (1), 479.

(50) Song, J.; Zhou, W. Multiresonant composite optical nano-antennas by out-of-plane plasmonic engineering. *Nano Lett.* **2018**, *18* (7), 4409–4416.

(51) Song, J.; Nam, W.; Zhou, W. Scalable high-performance nanolaminated SERS substrates based on multistack vertically oriented plasmonic nanogaps. *Adv. Mater. Technol.* **2019**, *4* (5), No. 1800689.

(52) Joo, T. H.; Kim, M. S.; Kim, K. Surface-enhanced Raman scattering of benzenethiol in silver sol. *J. Raman Spectrosc.* **1987**, *18* (1), 57–60.

(53) Le Ru, E. C.; Blackie, E.; Meyer, M.; Etchegoin, P. G. Surface enhanced Raman scattering enhancement factors: a comprehensive study. *J. Phys. Chem. C* **2007**, *111* (37), 13794–13803.

(54) Zeman, E. J.; Schatz, G. C. An accurate electromagnetic theory study of surface enhancement factors for silver, gold, copper, lithium, sodium, aluminum, gallium, indium, zinc, and cadmium. *J. Phys. Chem.* **1987**, *91* (3), 634–643.

(55) Knapp, E. W.; Fischer, S. F. On the theory of homogeneous and inhomogeneous line broadening. An exactly solvable model. *J. Chem. Phys.* **1981**, *74* (1), 89–95.

(56) Yu, Y.; Schletz, D.; Reif, J.; Winkler, F.; Albert, M.; Fery, A.; Kirchner, R. Influences on Plasmon Resonance Linewidth in Metal–Insulator–Metal Structures Obtained via Colloidal Self-Assembly. *ACS Appl. Mater. Interfaces* **2020**, *12* (50), 56281–56289.